

Warren Reid^{1,3} and Quentin Parker^{1,2,3}

¹Macquarie University, Sydney, Australia; ²Australian Astronomical Observatory
³Macquarie University centre for Astronomy, Astrophysics and Astrophotonics

We have extended our search for faint Planetary Nebulae (PNe) in the Large Magellanic Cloud (LMC) to include the outer 56 deg² not covered in the original UK Schmidt Telescope (UKST) survey of the central 25deg². Candidate PNe were selected for follow-up using the Magellanic Cloud Emission Line Survey (MCELS) and the UKST H α /SR LMC survey. With optical spectroscopy and near- and mid-infrared data, we have confirmed 61 new and 97 (of the 102) previously known PNe in the outer LMC. We find 5 previously known PNe to be other object types. This brings the number of currently confirmed LMC PNe to 715.

Introduction

In 2006 Reid & Parker added 460 planetary nebulae (PNe) to the 169 previously known across the central 25deg² of the LMC. These candidates were assigned a probability rating that relied on spectroscopic and optical confirmation. Assisted by high resolution spectroscopy and NIR imaging from Spitzer we have been able to either confirm or re-classify most of the lower ranked "possible" PNe. With candidate PNe found from MCELS and the UKST H α /SR survey we used AAOmega spectroscopy to verify and add 61 new PNe to the 97 previously known in the outer LMC (see Figure 1; Reid & Parker 2013). The brighter PN candidates were cross-checked against 2MASS (Cutri et al. 2003) NIR J (1.25 μ m), H (1.65 μ m) and K_s (2.16 μ m) band-passes. By then overlaying SAGE (Meixner et al. 2006) false colour images at 3.6, 4.5, 5.8, 8 and 24 μ m as well as supplementary WISE (Wright et al. 2010) bands at 3.4 and 4.6 μ m, we could assess the IR SEDs (Figures 2 and 3). The resulting large number of PNe now confirmed across the whole LMC (see figure 4 and 5) are yielding significant advances in our knowledge of PN abundances and the LMC's kinematic sub-structures such as rotation, inclination, transverse velocity. New PN radial velocities are currently being compared to other tracers such as emission-line stars, YSOs, HII regions and the HI gas disk. These are being used to verify LMC evolutionary models. Optical diagnostics (Figure 6) and mid-infrared colour-colour comparisons (Figure 7) purify object identification and allow us to compare PNe in the outer LMC with those on the main bar. Our new, improved method for deriving excitation class (Figures 8-10) allows more accurate analysis of the central stars while multi-wavelength PN luminosity functions (PNLFs) help to identify any population sub-trends or 'dips' while providing an accurate bright end, used as a standard candle (Figures 11 - 12).

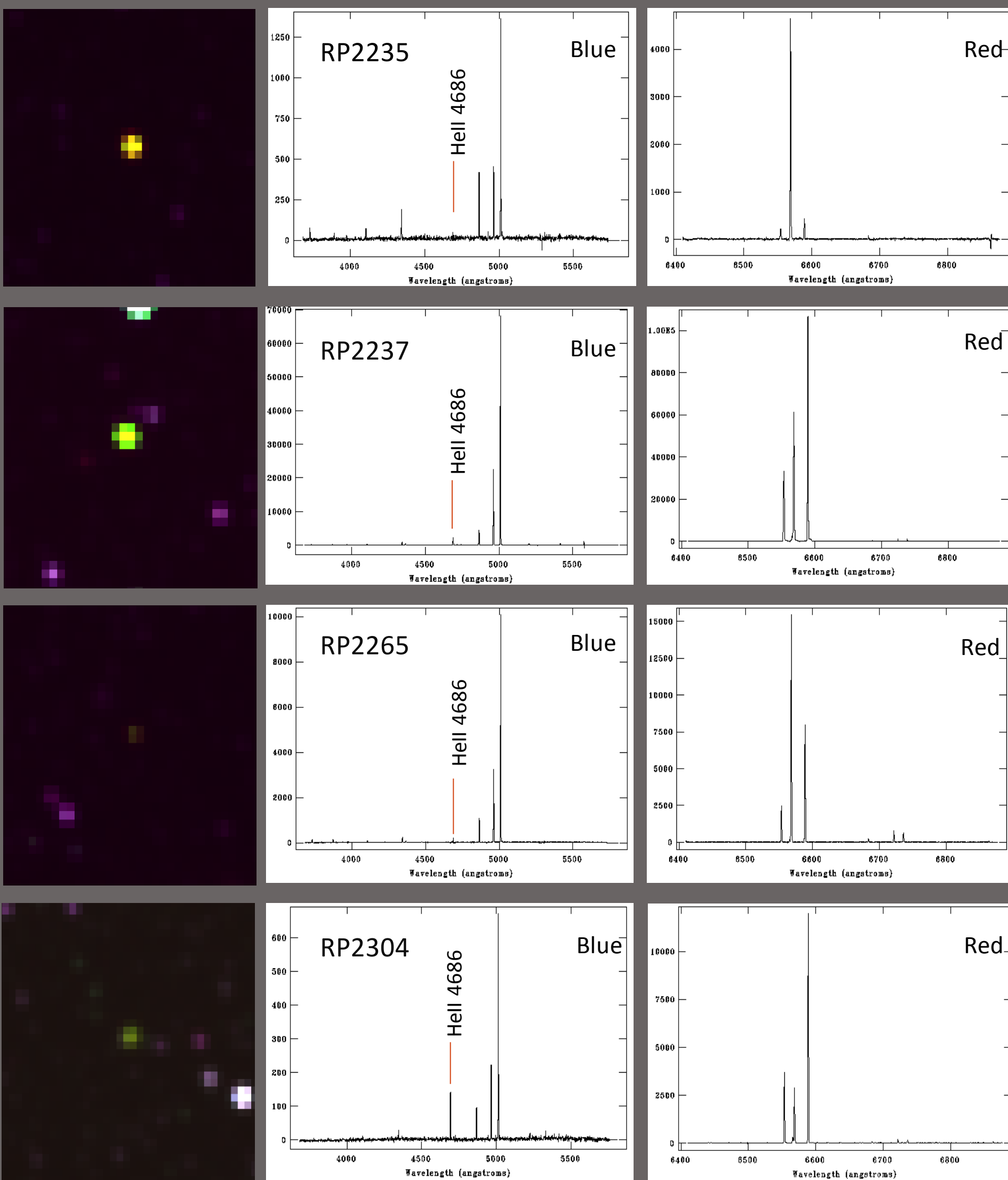


Figure 1. A representative sample of PNe in the LMC. Left: the image from MCELS. Middle: the confirmatory blue 580V spectrum from AAOmega. Right: the confirmatory red 1000R spectrum from AAOmega.

Multi-wavelength spectral energy distributions

By plotting the SEDs for objects known to be often confused with PNe we have a tool to help identify PN mimics. PNe containing dust components, emission lines, molecular lines and a central stellar source create a characteristic shape. Figure 2 shows the averaged SEDs for all 715 PNe in the LMC compared to an average for other object types also in the LMC. The subtle differences between the SEDs can be of enormous benefit when the low resolution optical spectra are inconclusive. The noticeable rise in the SEDs for previously known PNe around the V band (Figure 3 left) shows the strength of the [OIII] λ 5007 emission lines in these brighter objects compared to the more highly evolved and fainter PNe (Figure 3 right), which are generally have stronger [NII] emission.

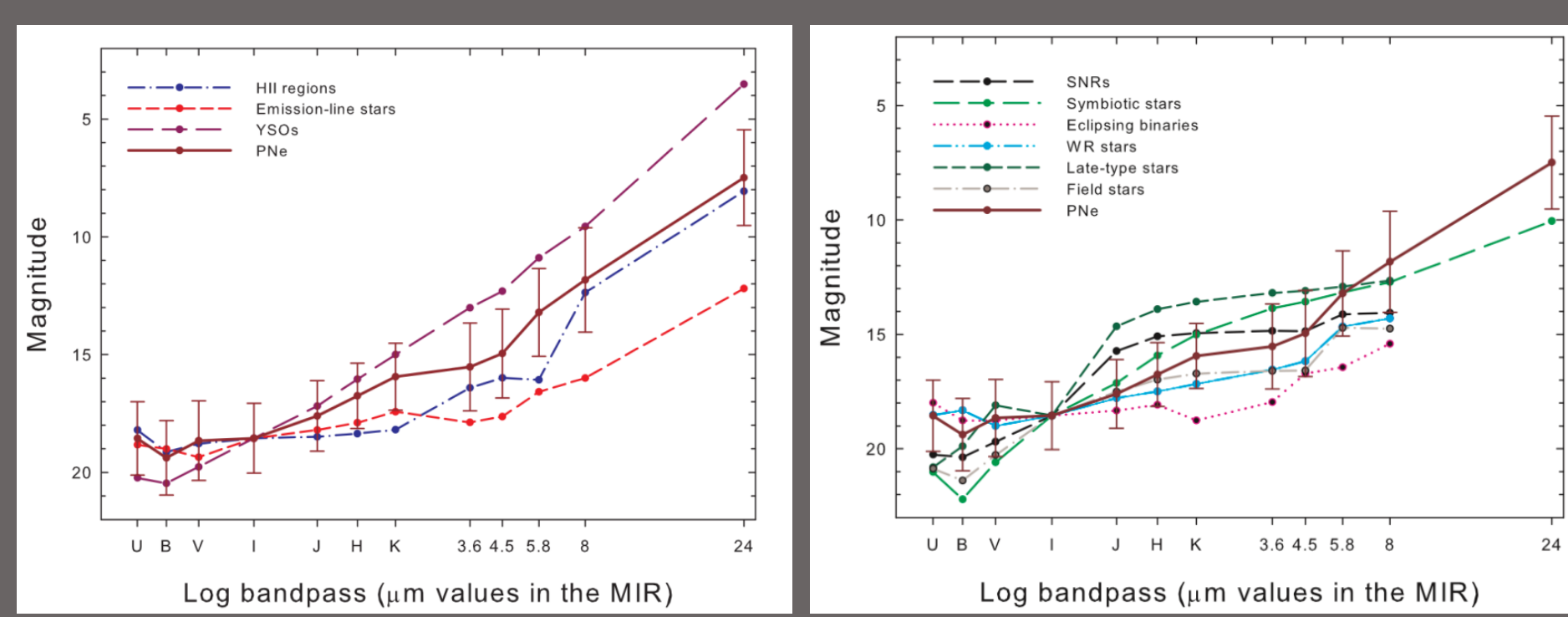


Figure 2. Left: The mean SEDs covering U band to 24 μ m in the MIR for HII regions emission-line stars and YSOs. These are the object types most commonly confused with PNe. The average fluxes are derived solely from LMC objects. The average for all LMC PNe is shown as a solid dark brown line with error bars. Objects are normalised to the mean PN magnitude of 18.85 in the I band. Right: The same but for SNRs, symbiotic stars, eclipsing binaries, WR stars, late-type stars and field stars.

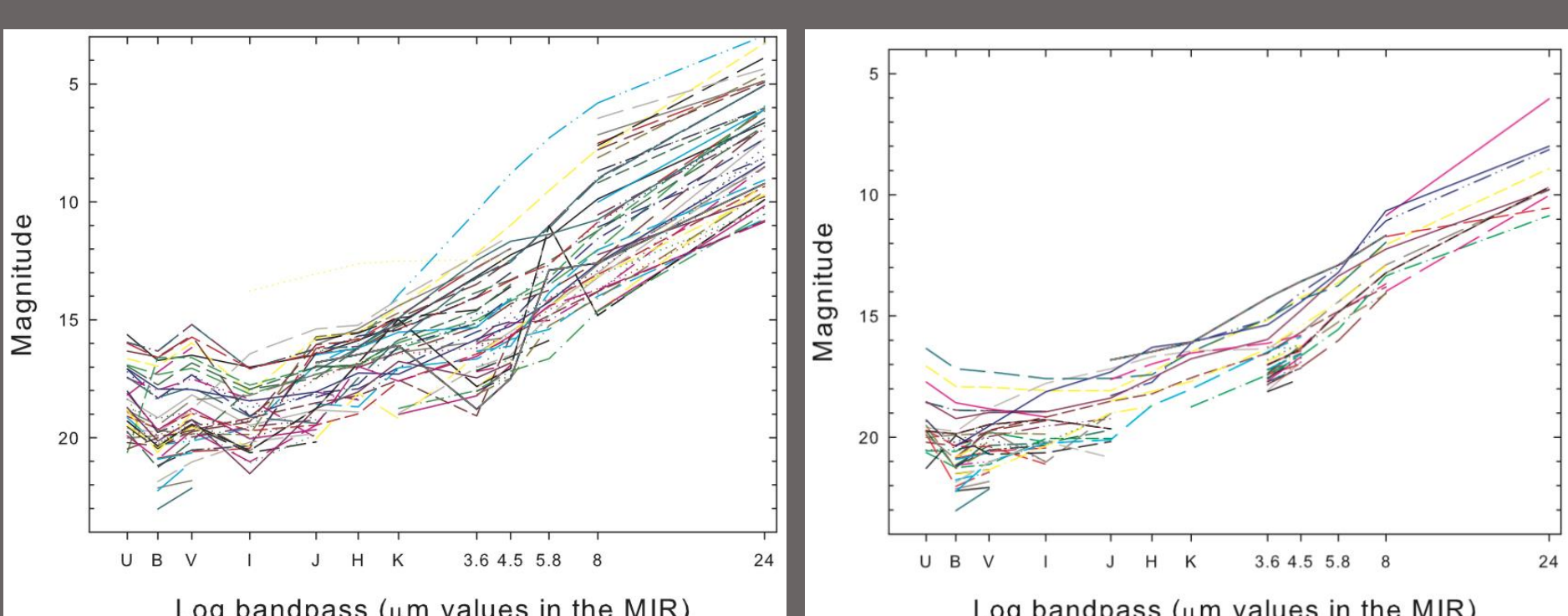


Figure 3. Left: The SED covering U band to 24 μ m for all previously known PNe in the outer LMC where data linking at least two consecutive points are available. Right: The same but for all the newly identified PNe in the outer LMC.

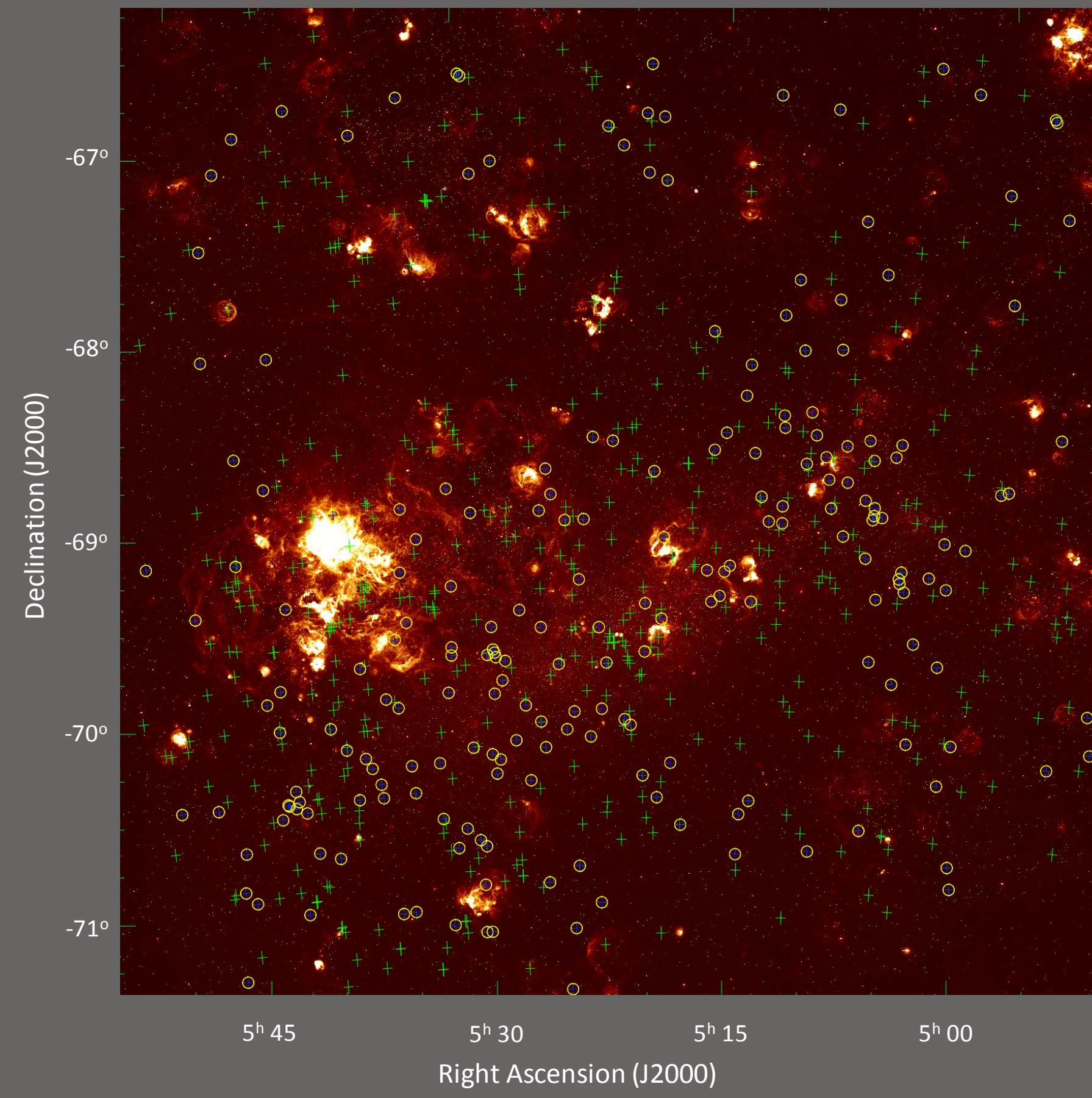


Figure 4. The UKST H α image of the LMC with Type I PNe shown as a blue cross within a yellow circle and non-Type I PNe are shown as green crosses. Type I PNe in the LMC are defined by $(\text{He}/\text{H}) > 0.10$ and $(\text{N}^+/\text{O}^+) > 0.25$.

Optical diagnostics

Basic diagnostic plots (eg. Figure 6) provide an overall snapshot of line characteristics and ratios, useful for identifying PN mimics. However, considerable overlap between regions occupied by PNe, HII regions, symbiotic stars, WR stars, AGB stars, SNRs and AGNs means that there remains a heavy reliance on follow-up assessment using individual spectra, multi-wavelength analysis & high-resolution optical imaging.

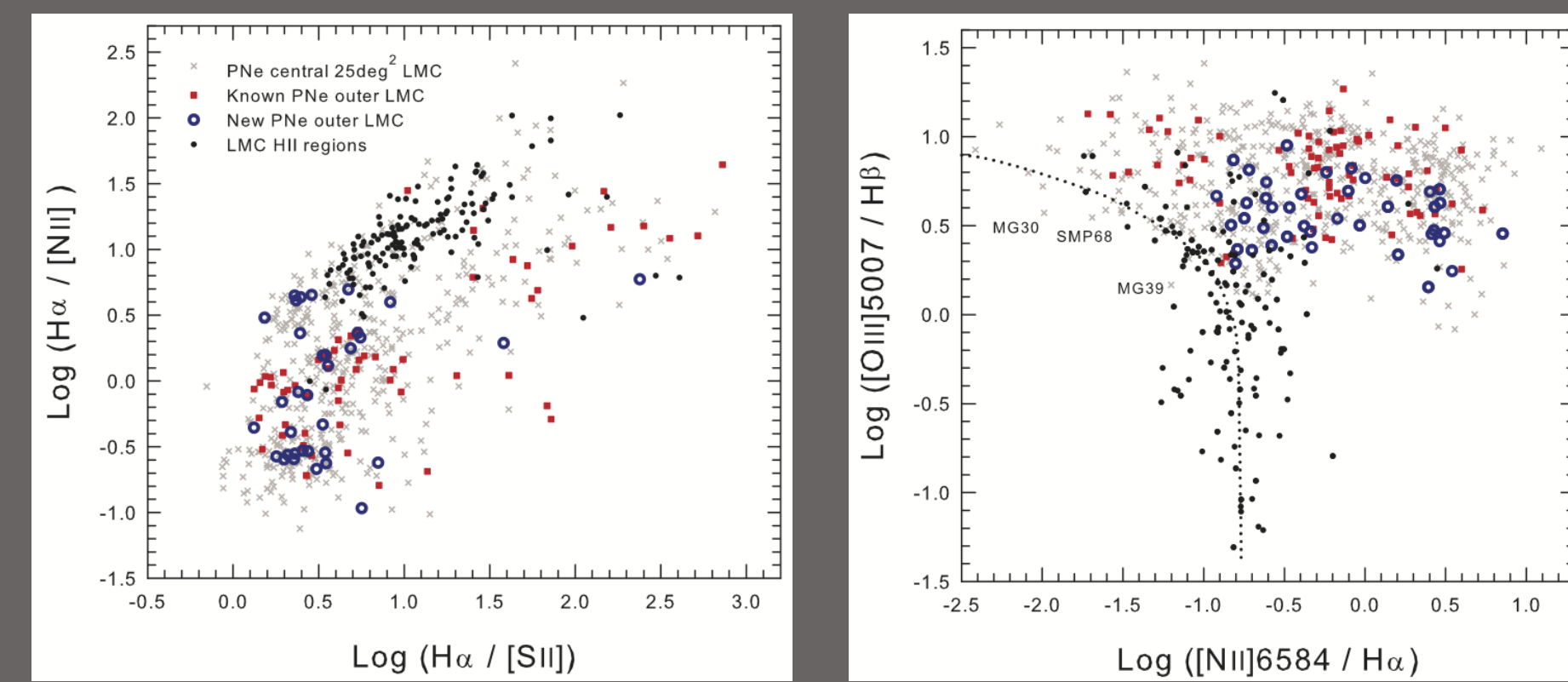


Figure 6. Left: The $\log(\text{H}\alpha/([\text{NII}]6583+6548))$ versus $\log(\text{H}\alpha/([\text{SII}]6716+6731))$ diagnostic diagram. PNe within the central 25deg² main bar region of the LMC are marked as grey crosses, previously known PNe in the outer LMC are marked as red squares and the newly discovered PNe in the outer LMC are marked as blue circles. HII regions are shown as filled black circles. Right: the same but for $\log([\text{OIII}]5007/\text{H}\beta)$ versus $\log([\text{NII}]6583/\text{H}\alpha)$. The black broken line is the line of best fit for HII regions in the LMC.

Mid-infrared comparisons

By plotting various MIR bands (eg. Figure 7), we can see trends and outlying objects that give us information regarding the strength and likely composition of the dust, temperature and other features. In Figure 7, PNe with $[8]-[24] < 3$ represent some of the smallest and faintest PNe in the LMC. With the exception of SMP11, which is a very young PN, all have very low H α emission. MG47 is a very small, high excitation PN with low [NII] and [SII]. Its position indicates a lack of [NeV] and dust continuum at [24].

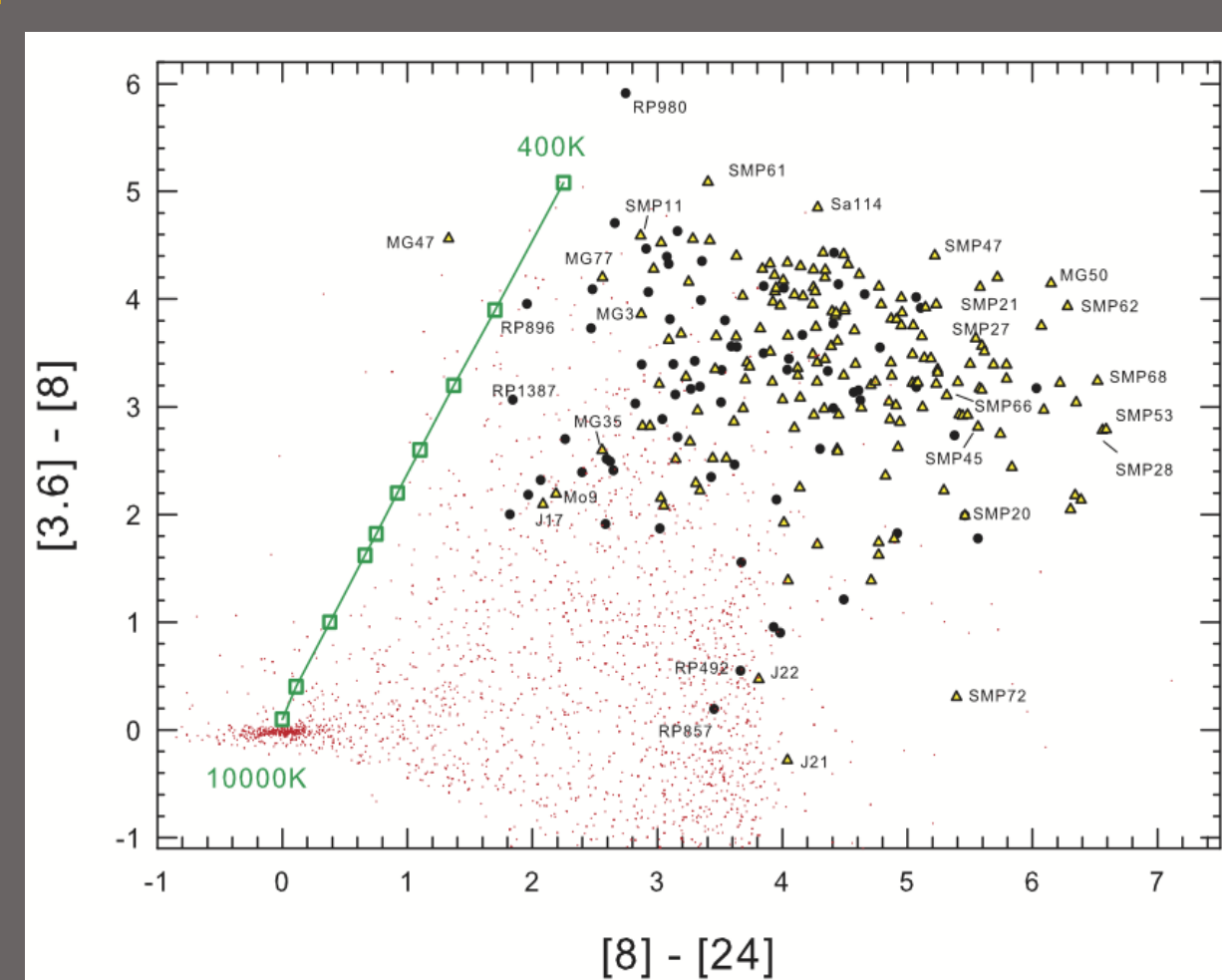


Figure 7. The $[3.6]-[8]$ versus $[8]-[24]$ colour-colour diagram. Blackbody temperatures are plotted as connecting squares at 400K, 500K, 600K, 700K, 800K, 900K, 1000K, 1500K, 3000K and 10,000K. Previously known PNe are shown as triangles and RP PNe are black circles.

Excitation class for the inner and outer LMC

We use our updated method (Exp) to compare the excitation class of PNe in the central 25deg² with those in the outer LMC (figures 8, 9, 10) including recently discovered PNe.

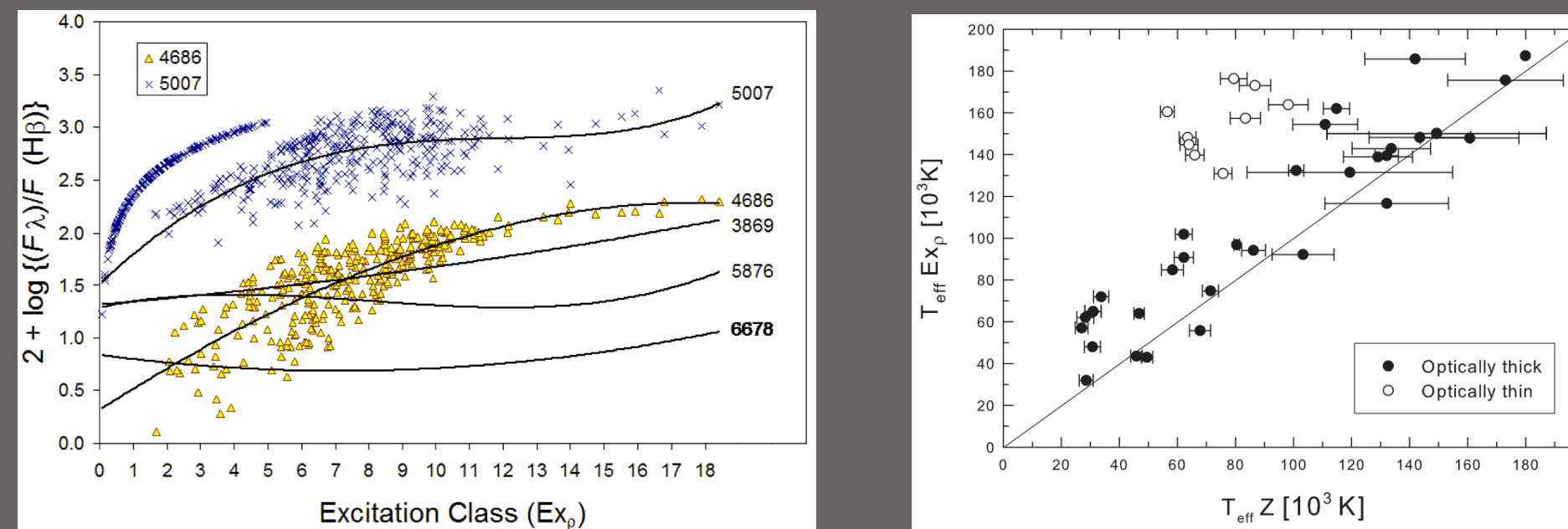


Figure 8. The position of 5 key emission line fluxes with respect to H β sensitive to excitation class. Fluxes for [OIII] λ 5007 and HeII λ 4686 have been plotted together with a polynomial trend line of best fit for each line. Figure 9. Temperatures using the Zanstra method (Villaver et al. 2003) are plotted against those found from the excitation class. In addition, $T_{\text{eff}}(\text{HeII})/T_{\text{eff}}(\text{H}\beta) \sim 2$ indicates optically thin nebulae.

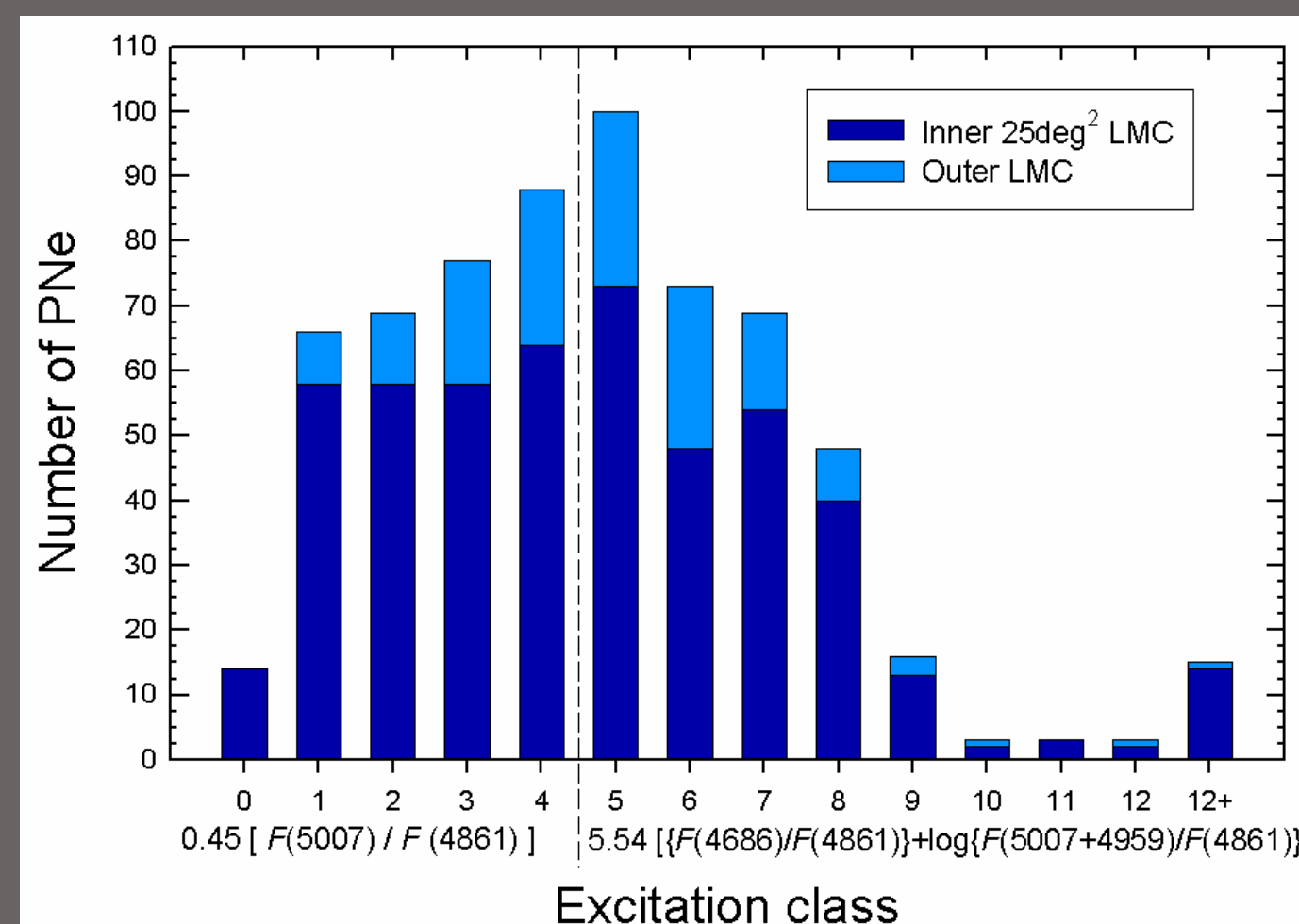


Figure 10. The excitation class (Exp) comparing PNe in the inner and outer LMC. A broken line separates the equation used for deriving low excitation class from that used to derive medium to high excitation classes.

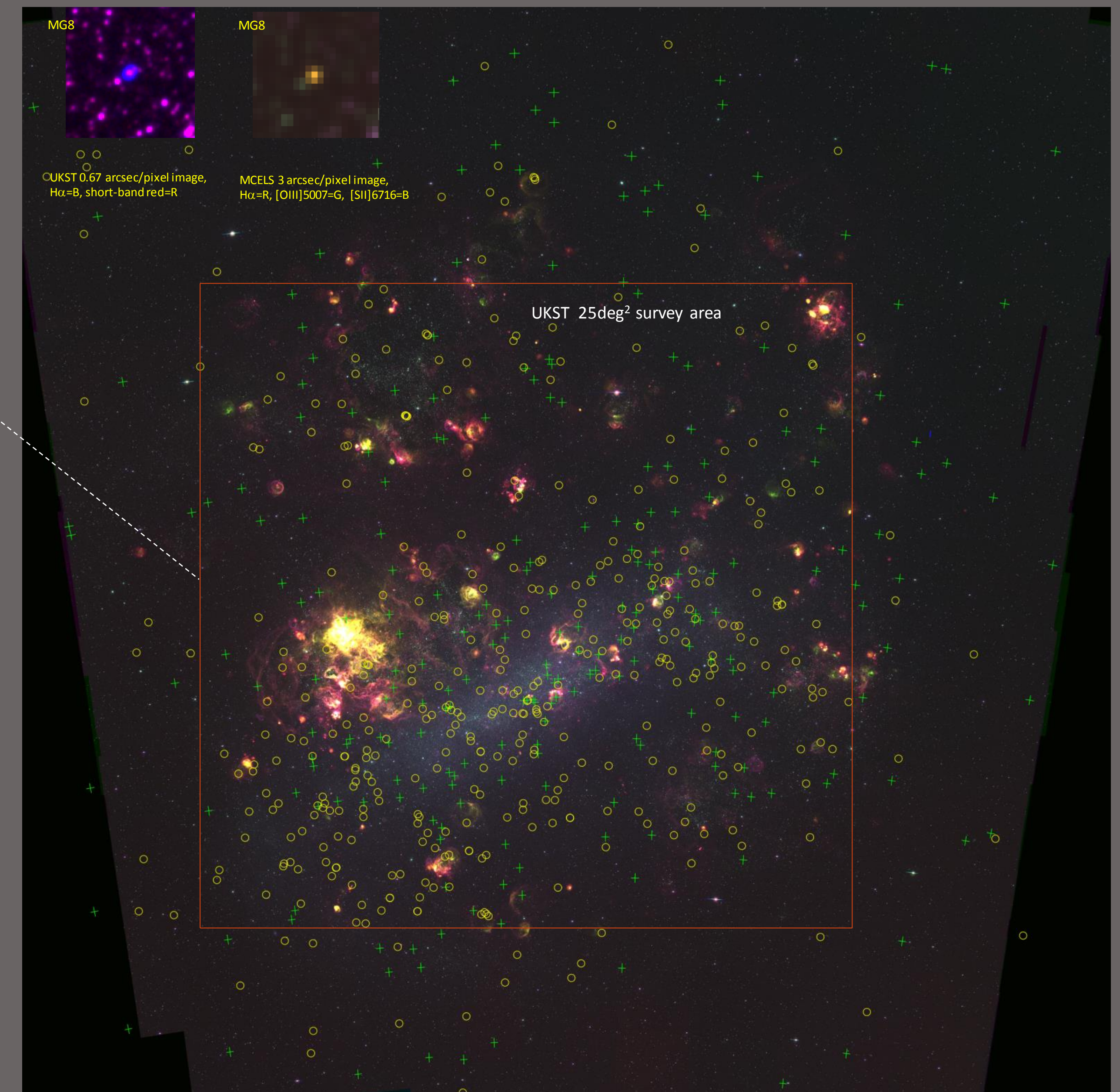


Figure 5. MCELS colour composite image of the LMC where $R = \text{H}\alpha$, $G = [\text{OIII}]5007$, $B = [\text{SII}]6716,6731$. Previously known PNe are shown as yellow circles and newly discovered PNe are shown as green crosses.

New PNLF covering the entire LMC

Our confirmation of all previously known and new PNe to $V=22$ provides the most accurate PNLF ever achieved across a whole galaxy. This new, updated PNLF including all the previously known and recently discovered PNe in the outer LMC can accurately predict the number of stars at each evolutionary stage compared to the luminosity and mass of the whole galaxy. This is not attainable for any galaxies other than the LMC and SMC, as dust obscures too much of our own Galaxy and other galaxies are too distant to identify faint PNe. Our new LMC PNLF is for a much more complete sample in terms of depth, coverage and PNe evolutionary state covering an unprecedented 10 magnitude range (see RP for details about the central main bar region).

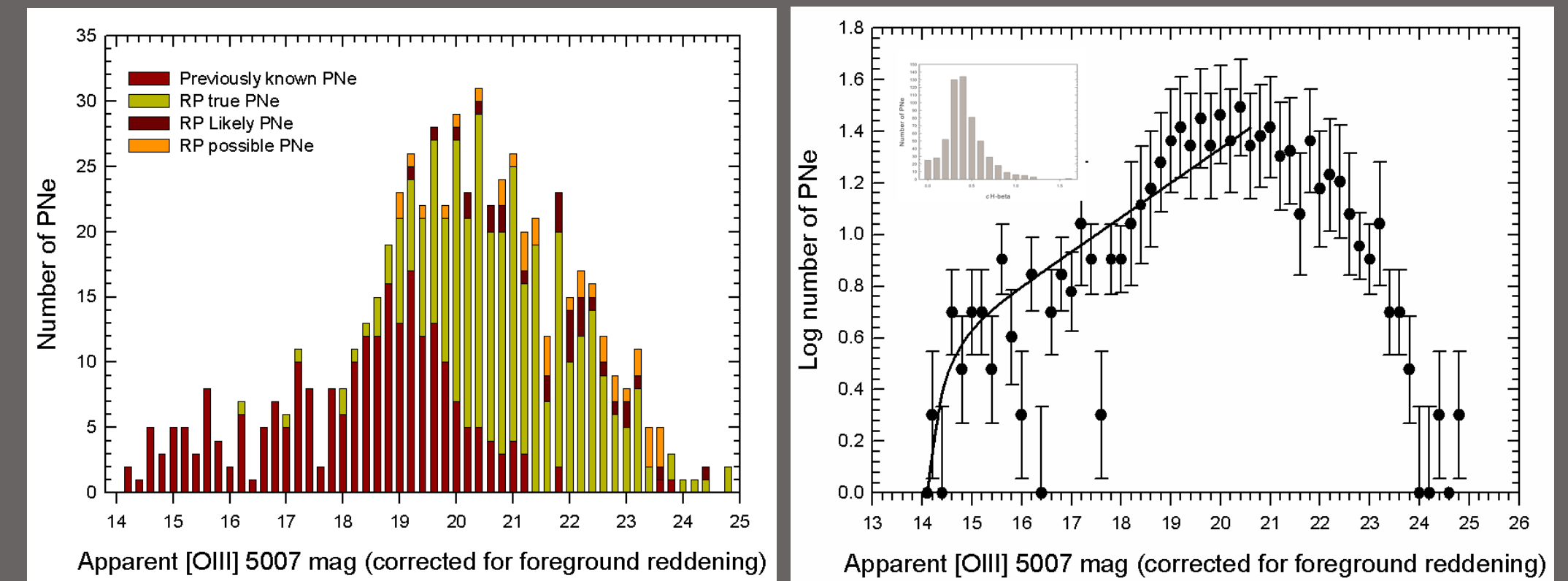


Figure 11a. The PNLF for the entire LMC, derived from a homogeneous sample of previously known and RP PNe. The bins have been stacked in order to show the relative number of previously known, true, likely and possible PNe. Figure 11b. In order to use the PNLF for distance determination, the data have only been corrected for line of sight reddening. The magnitudes have been binned into 0.2 mag intervals and plotted in log space. The solid line is the log of the truncated exponential curve, as predicted by Ciardullo et al. (1989) convolved for errors and placed at the best-fit position at the bright end of the observed function. Poisson error bars are included. It is assumed that the decreasing number of objects at magnitudes $m_{5007} > 21$ is due to incompleteness. This provides the first, direct estimation of M_V for [OIII] λ 5007 in the LMC using a 3.4 magnitude range at the bright end of the LMC PNLF. The insert shows the overall extinction based on the Balmer decrement.

To estimate the distance, we use the χ^2 method to fit a truncated exponential curve to the observed PNLF corrected for foreground reddening (Figure 11a). The bright cut-off absolute magnitude M_V has been estimated as $M_V = -4.44 \pm 0.05$ (Ciardullo et al. 1989, 2002; Jacoby et al. 1992). We adopt this value because it reflects the theoretical dependence of M_V on metallicity (Dopita et al. 1992) and enables us to make a direct comparison to previous LMC PNLF distance estimates. This gives us a distance modulus of 18.46 ± 0.2 for the LMC where the magnitude errors are used as systematic uncertainties for the distance modulus.

LMC PNLF in the mid-infrared

Since the mechanisms leading to MIR emission in PNe are complex and varied, luminosity functions built on the SAGE bands will each be the result of different components such as PAHs, line radiation, optically thin thermal dust emission, Q-branches of various hydrocarbon molecules and emission from forbidden lines. There is no obvious reason why these functions should correlate to the standard PNLFs built on the [OIII] λ 5007 and H β lines, which loosely trace stellar temperature, excitation and metallicity. Nor should they necessarily correlate to the truncated exponential curve (Ciardullo et al. 1989). Nonetheless, there are forbidden emission lines and optically thin thermal dust emission that are linked to the UV luminosity of the central star. MIR PNLFs may therefore track UV flux in bands where these components dominate.

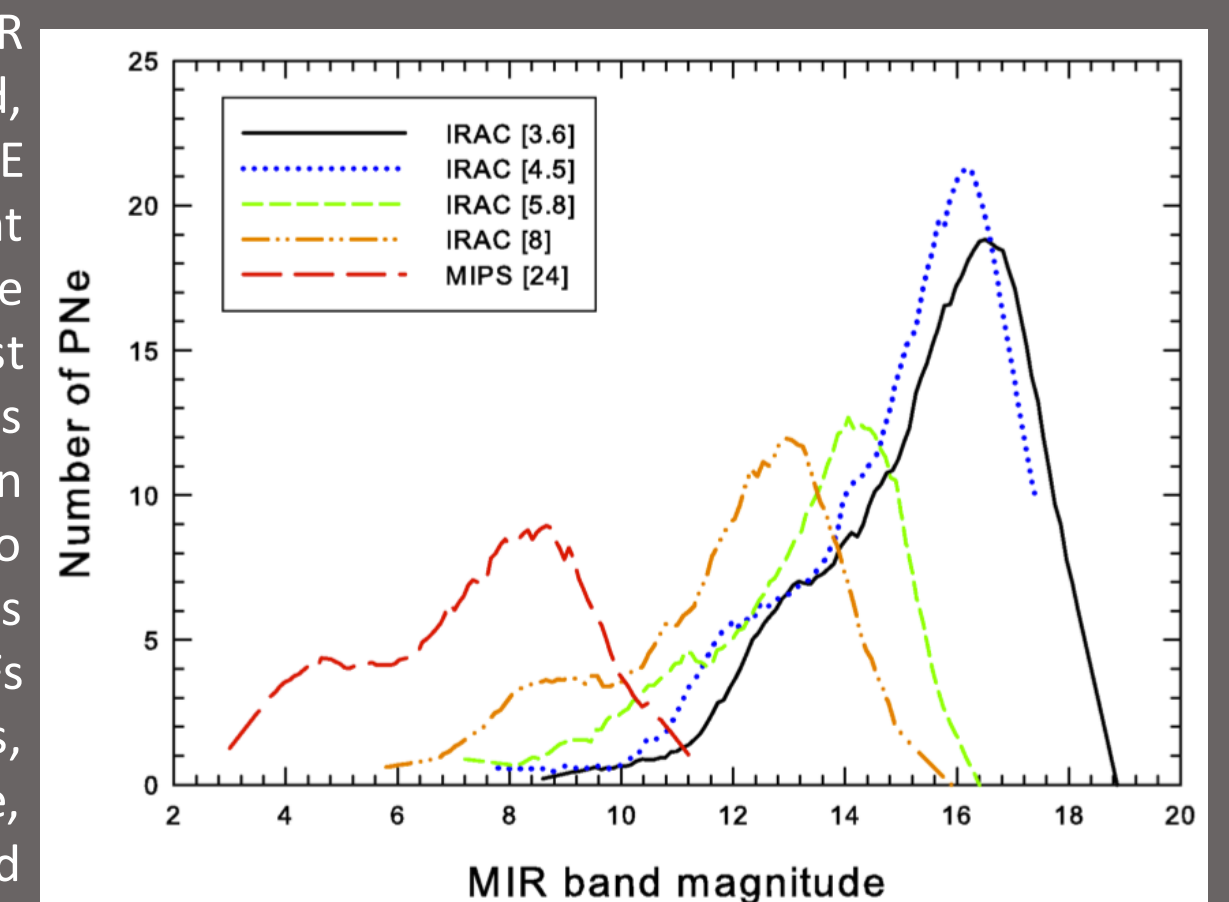


Figure 12. Luminosity functions for the [3.6], [4.5], [5.8], [8] IRAC bands and the [24] MIPS band. The number of detected objects decreases as a function of the cutoff in instrumental sensitivity. A noticeable 'hump' and 'dip' at the bright end becomes proportionally more prominent at longer wavelengths.

References

- Ciardullo R., Jacoby G., Ford H.C., Neill J.D., 1989 ApJ, 339, 53
- Ciardullo R., et al. 2002 ApJ, 577, 31
- Cutri R.M., et al. 2003, www.ipac.caltech.edu/2mass/releases
- Dopita M.A., Jacoby G.H., Vassiliadis E., 1992 ApJ, 389, 27
- Jacoby G.H., et al. 1992 PASP, 104, 599
- Meixner M., et al. 2006 AJ, 132, 2268
- Reid W.A. and Parker Q.A., 2006 MNRAS, 373, 521
- Reid W.A. and Parker Q.A., 2010 (RPA) MNRAS, 405, 1349
- Reid W.A. and Parker Q.A., 2010 (RPA) PASA, 27, 187
- Reid W.A. and Parker Q.A., 2013 MNRAS, temp 2374
- Smith R.C. and the MCELS team, 1998 PASA 15, 163
- Villaver E., Stanghellini L., Shaw R.A., 2003 ApJ, 597, 298
- Wright E.L., et al. 2010 AJ, 140, 1868

Although PNe were allotted to 0.25 mag bins for the MIR PNLFs shown in Figure 12, we show a line of best fit in order to facilitate the comparison. There is a clear change in the shape of the bright end with increasing wavelength. The dip gradually becomes more dominant and moves closer to the bright cut-off with increasing wavelength. This dip represents a point of rapid evolution of the central star. The change corresponds to an increase in the 'hump' or clumping of PNe gathering at the bright end.